2022-12

ROCKY BOTTOM ROUGHNESS ALONG THE CALIFORNIA COAST

Dressel, Stefanie M.

Monterey, CA; Naval Postgraduate School

NAVAL POSTGRADUATE SCHOOL

MONTEREY, CALIFORNIA

THESIS

ROCKY BOTTOM ROUGHNESS ALONG THE CALIFORNIA COAST

by

Stefanie M. Dressel

December 2022

Thesis Advisor: James H. MacMahan
Second Reader: Edward B. Thornton

Approved for public release. Distribution is unlimited.

THIS PAGE INTENTIONALLY LEFT BLANK

REPORT DOCUMENTATION PAGE	*Form Approved OMB No. 0704-0188*

Public reporting burden for this collection of information is estimated to average 1 hour per response, including the time for reviewing instruction, searching existing data sources, gathering and maintaining the data needed, and completing and reviewing the collection of information. Send comments regarding this burden estimate or any other aspect of this collection of information, including suggestions for reducing this burden, to Washington headquarters Services, Directorate for Information Operations and Reports, 1215 Jefferson Davis Highway, Suite 1204, Arlington, VA 22202-4302, and to the Office of Management and Budget, Paperwork Reduction Project (0704-0188) Washington, DC 20503.

1. AGENCY USE ONLY *(Leave blank)*	**2. REPORT DATE** December 2022	**3. REPORT TYPE AND DATES COVERED** Master's thesis

4. TITLE AND SUBTITLE
ROCKY BOTTOM ROUGHNESS ALONG THE CALIFORNIA COAST

5. FUNDING NUMBERS
N0001422WX01015

6. AUTHOR(S) Stefanie M. Dressel

7. PERFORMING ORGANIZATION NAME(S) AND ADDRESS(ES)
Naval Postgraduate School
Monterey, CA 93943-5000

8. PERFORMING ORGANIZATION REPORT NUMBER

9. SPONSORING / MONITORING AGENCY NAME(S) AND ADDRESS(ES)
ONR, Arlington, VA 22203

10. SPONSORING / MONITORING AGENCY REPORT NUMBER

11. SUPPLEMENTARY NOTES The views expressed in this thesis are those of the author and do not reflect the official policy or position of the Department of Defense or the U.S. Government.

12a. DISTRIBUTION / AVAILABILITY STATEMENT
Approved for public release. Distribution is unlimited.

12b. DISTRIBUTION CODE
A

13. ABSTRACT (maximum 200 words)

The roughness of ninety-nine rocky bottoms is measured for nearshore bathymetric surveys (depths >5m to several km offshore) resolved at 1 or 2m extending the length of California. Visual inspection shows a wide variety of rock formations comprising the bottoms. Many flat areas are found in depressions amongst the rocks that presumably are filled with sediments. Roughness is measured as the standard deviation of the residual elevation, σ_z, about a mean planform that is averaged over 750m in the alongshore and cross-shore. The σ_z vary from 0.35m to 8.6m with a mean of 2.1m. The measured rocky bottoms are significantly rougher than previously measured coral reef bottoms. Roughness scale is determined from ensemble-averaged wavenumber (k) spectra of elevation, $\widehat{G_{zz}}(k)$, and of bottom slopes, $\widehat{G_{\beta\beta}}(k)$ in both the cross-shore (x) and alongshore (y). All $\widehat{G_{zz}}(k)$ are red with maximum variance at low wavenumber with slopes increasing from -1 to -3, have similar shapes, and appear near isotropic in x and y. Assuming a power law relationship in k, the slopes of $\widehat{G_{zz}}(k)$, denoted as $\widehat{\alpha_z}(k)$, are shown to be related to the slopes of $\widehat{G_{\beta\beta}}(k)$, denoted as $\widehat{\alpha_\beta}(k)$, by $log\ \widehat{\alpha_\beta}(k) = log\ \widehat{\alpha_z}(k)$ +2 in x and y. Both $\widehat{\alpha_z}(k)$ and $\widehat{\alpha_\beta}(k)$ are isotropic in x and y evidenced by their 95% confidence intervals overlapping across the intermediate wavenumber scales <1/666m.

14. SUBJECT TERMS bottom roughness, rocky bottom, rocky, rough	**15. NUMBER OF PAGES** 53
	16. PRICE CODE

17. SECURITY CLASSIFICATION OF REPORT	**18. SECURITY CLASSIFICATION OF THIS PAGE**	**19. SECURITY CLASSIFICATION OF ABSTRACT**	**20. LIMITATION OF ABSTRACT**
Unclassified	Unclassified	Unclassified	UU

NSN 7540-01-280-5500

Standard Form 298 (Rev. 2-89)
Prescribed by ANSI Std. 239-18

THIS PAGE INTENTIONALLY LEFT BLANK

Approved for public release. Distribution is unlimited.

ROCKY BOTTOM ROUGHNESS ALONG THE CALIFORNIA COAST

Stefanie M. Dressel
Lieutenant Commander, United States Navy
BS, Old Dominion University, 2011
MBA, University of Florida, 2020

Submitted in partial fulfillment of the
requirements for the degree of

MASTER OF SCIENCE IN METEOROLOGY AND PHYSICAL OCEANOGRAPHY

from the

NAVAL POSTGRADUATE SCHOOL
December 2022

Approved by: James H. MacMahan
Advisor

Edward B. Thornton
Second Reader

Peter C. Chu
Chair, Department of Oceanography

THIS PAGE INTENTIONALLY LEFT BLANK

ABSTRACT

The roughness of ninety-nine rocky bottoms is measured for nearshore bathymetric surveys (depths >5m to several km offshore) resolved at 1 or 2m extending the length of California. Visual inspection shows a wide variety of rock formations comprising the bottoms. Many flat areas are found in depressions amongst the rocks that presumably are filled with sediments. Roughness is measured as the standard deviation of the residual elevation, σ_z, about a mean planform that is averaged over 750m in the alongshore and cross-shore. The σ_z vary from 0.35m to 8.6m with a mean of 2.1m. The measured rocky bottoms are significantly rougher than previously measured coral reef bottoms. Roughness scale is determined from ensemble-averaged wavenumber (k) spectra of elevation, $\widehat{G_{zz}}(k)$, and of bottom slopes, $\widehat{G_{\beta\beta}}(k)$ in both the cross-shore (x) and alongshore (y). All $\widehat{G_{zz}}(k)$ are red with maximum variance at low wavenumber with slopes increasing from -1 to -3, have similar shapes, and appear near isotropic in x and y. Assuming a power law relationship in k, the slopes of $\widehat{G_{zz}}(k)$, denoted as $\widehat{\alpha_z}(k)$, are shown to be related to the slopes of $\widehat{G_{\beta\beta}}(k)$, denoted as $\widehat{\alpha_\beta}(k)$, by $log\ \widehat{\alpha_\beta}(k) = log\ \widehat{\alpha_z}(k)$ +2 in x and y. Both $\widehat{\alpha_z}(k)$ and $\widehat{\alpha_\beta}(k)$ are isotropic in x and y evidenced by their 95% confidence intervals overlapping across the intermediate wavenumber scales <1/666m.

THIS PAGE INTENTIONALLY LEFT BLANK

TABLE OF CONTENTS

I. INTRODUCTION 1

II. METHODS-DATA PREPARATION 5

A. HIGH-RESOLUTION BATHYMETRY 5

B. INTERMEDIATE-SCALE, O(10-1000M), MORPHOLOGY 7

1. Local Coordinate Frame Transformation 7

2. Intermediate-Scale Bathymetry 8

3. Selecting Representative Rocky Bottoms 11

III. RESULTS 13

IV. DISCUSSION 21

A. BOTTOM ROUGHNESS 21

B. WAVENUMBER SPECTRA OF Z' 22

C. BOTTOM SLOPE WAVENUMBER SPECTRA 23

D. FOURIER MODEL OF BOTTOM ROUGHNESS 24

V. CONCLUSION 29

LIST OF REFERENCES 31

INITIAL DISTRIBUTION LIST 35

THIS PAGE INTENTIONALLY LEFT BLANK

LIST OF FIGURES

Figure 1. Locations of bathymetry and rocky bottom subsets 6

Figure 2. Monterey Peninsula Principal Component Analysis (PCA) 8

Figure 3. Bathymetry of Cypress Point to Point Pinos, Monterey Peninsula 10

Figure 4. Rocky bottom slopes in the alongshore and cross-shore directions 12

Figure 5. Standard deviations of z' and β by latitude and histograms of $\sigma_{z'}$ and σ_{β} 13

Figure 6. Linear regression of σ_{β} with $\sigma_{z'}$ 14

Figure 7. Distributions of z' and bottom slopes 15

Figure 8. Average spectra and spectral slopes of z' and bottom slope of rocky bottoms 18

Figure 9. Histogram of the ratio of the standard deviations in x- and y-directions 19

Figure 10. Rocky bottom elevation (z') and bottom slopes (β) of Yankee Point 22

Figure 11. Transfer function of the spectral slope 26

Figure 12. Wave bottom interactions 27

THIS PAGE INTENTIONALLY LEFT BLANK

LIST OF TABLES

Table 1. Roughness as measured by standard deviation about the mean profile, $\sigma_{z'}$, and spectral wavenumber slope, α_z. 2

Table 2. Rocky bottom statistics 16

THIS PAGE INTENTIONALLY LEFT BLANK

LIST OF ACRONYMS AND ABBREVIATIONS

α	spectral slope
ASCII	American Standard Code for Information Interchange
β	slope
β_x	bottom slope in the cross-shore
β_y	bottom slope in the alongshore
cm	centimeter
Cf	bottom shear stress coefficient
CSMP	California Seafloor Mapping Program
CSUMB	California State University Monterey Bay
e_{30}	easting associated with 30m isobath
f_e	energy friction factor
$\hat{G}$	normalized energy density spectra
k	wavenumber
KGPS	kinematic global positioning system
km	kilometer
L	bathymetric length scales
m	meter
MHHW	Mean Higher High Water
MLLW	Mean Lower Low Water
n_{30}	northing associated with 30m isobath
NAD 83	North American Datum of 1983
NAVD 88	North American Vertical Datum of 1988
O	on the order of
PCA	Principal Component Analysis
PDF	Probability Density Function
SFML	Seafloor Mapping Laboratory
σ_β	standard deviation of bottom slope

$\sigma_{z'}$	standard deviation of elevation
std. dev.	standard deviation
θ_{30}	rotation angle
UAV	unmanned aerial vehicle
USGS	United States Geological Survey
UTM	Universal Transverse Mercator
z	elevation
z’	deviation of bottom surface (demeaned elevation)
z_0	hydraulic roughness

ACKNOWLEDGMENTS

The author would like to thank the Oceanography Department of the Naval Postgraduate School for their support in conducting this research. Dr. Edward Thornton, Dr. James MacMahan, and Mike Cook were instrumental in the completion of this thesis. This work would not be possible without Carrie Bretz and the data provided by California State University Monterey Bay. This work was funded by the Office of Naval Research under Grant No. N0001422WX01015.

THIS PAGE INTENTIONALLY LEFT BLANK

I. INTRODUCTION

About 75% of the world's coastlines can be described as rocky (Bird, 2011). Gon et al. (2020) defines the rocky shore as "quasi-random undulations of rock mounds or platforms that result in quick transitions between bathymetric highs and lows". They further divide rocky shores into categories, including sub- and intertidal rocky reefs and rocky platforms. Rocky shores as a defined habitat have also been the focus of marine biological studies (e.g., Witman & Dayton, 2001). Rocky platforms are near planar beaches composed of relatively flat erodible rock comprising about 20% of rocky shores (Kirk, 1977; Emery and Kuhn, 1982; Trenhaile, 2002). To date, only Poate et al. (2018) explored the wave transformation on a few rocky shore platforms. And to date, only Gon et al. (2020) explored wave transformation across rocky reef seaward of the surf zone. To our knowledge, there has been no detailed quantification of the subaqueous rough bottoms of rocky reefs. The objective of this study is to characterize the roughness of the subaqueous rocky bottom for application to wave and current studies.

Ardhuin et al. (2003) summarized the different processes for swell-sea waves due to bottom variability at different bathymetric length scales, L (see Fig. 1 in Ardhuin et al., 2003). Refraction and shoaling of waves are described by large-scale (L>750 m) bathymetry associated with mild bottom slopes. The effects of intermediate-scale (750m>L>1m) bottom variability are described with wave–bottom Bragg (forward) scattering theory (Hasselmann and Collins, 1968; Long, 1973; Ardhuin and Herbers, 2002; Ardhuin et al., 2003). The effect of small-scale roughness elements (1m>L>0.1m) is to enhance wave energy dissipation (Grant and Madsen, 1982; Nielsen, 1992; Soulsby, 1997). On sandy shores with O(cm) ripple roughness, bottom friction only causes significant wave attenuation over distances of O(10 km) (e.g., Ardhuin et al. 2003). On rougher topography, such as coral reefs, bottom friction induces large wave dissipation in shorter distances, significantly impacting wave transformation (Lowe et al., 2005; Monismith et al., 2015; Lentz et al., 2016). Gon et al. (2020) found significant wave dissipation owing to bottom friction over a short distance on a rocky reef. They found

energy friction factors, f_e, ranging from 4 to 34 that are larger than previously measured f_e on coral reefs and three orders of magnitude greater than on sandy beaches.

Coral reefs have rough bottoms and have been well-studied in recent years (Rogers et al., 2018; Duvall et al., 2019; amongst others). Although coral reef bottoms are generally not as rough as rocky bottoms (Gon et al., 2020), considerable insight can be gained from the knowledge obtained on coral reefs. Roughness metrics that have been commonly used to describe elevation variations about a mean profile (z') include the standard deviation, $\sigma_{z'}$, the ratios of physical length scales (rugosity), and topographic variation with spatial scale (wavenumber spectra) (Duvall et al., 2019). It was found for coral reefs $\sigma_{z'}$ ranged from 0.03 to 0.99m (Table 1) (Nunes and Pawlak, 2008; Jaramillo and Pawlak, 2011; Rogers et al., 2018; Duvall et al., 2019, 2020), which are smaller than 0.9m found by Gon et al. (2020) on a rocky reef.

Table 1. Roughness as measured by standard deviation about the mean profile, $\sigma_{z'}$, and spectral wavenumber slope, α_z.

Morphology/ Author	Area	Resolution Technique	$\sigma_{z'}$ (m)	α_z
Rocky Bottom Current Paper	California Coast 99-(~860m x1345m)	1m or 2m Sidescan sonar	0.35-8.6 mean 2.1	-1 to -3
Rocky Bottom Gon et al. (2020)	Hopkins Marine Station, CA (100m x150m)	1m Sidescan sonar	0.9	
Coral Reef Nunes and Pawlak (2008)	Honolulu, HI 1100-(12.5m lines)	10cm sonar		-3.0+/-0.7
Coral Reef Jaramillo and Pawlak (2011)	Honolulu, HI (6m x 6m)	~10cm UAV sidescan sonar	0.03-0.07	-0.89 to -1.73
Coral Reef Rogers et al. (2018)	Ofu, Samoa 12-(~24m x 32m)	10-30cm UAV video	0.15-0.5	~-2
Coral Reef Duvall et al. (2019)	Moorea, French Polynesia (256m x1000m)	1m Topographic lidar	0.22-0.99	-0.76, -1.12, -2
Coral Reef Duvall et al. (2020)	Moorea, French Polynesia 3-(10m x10m)	1cm Rotating scan sonar	0.16-0.27	-1.44, -1.68, -1.78

Based on the studies of coral reefs, Rogers et al. (2018) argued that for the expected rough, turbulent flow, form drag dominates the bottom friction. Form drag is characterized by the hydraulic roughness, $z_0 = f(z', dz'/dx)$), where z' is a measure of bottom roughness and dz'/dx is a measure of bottom slope. Both z' and bottom slope were described at scale by wavenumber spectra over coral reefs (Nunes and Pawlak, 2008; Jaramillo and Pawlak, 2011; Rogers et al., 2018; Duval et al., 2019, 2020). It was found that the wavenumber spectra could be generally described in terms of a power law, $G_{z'}(k) = Ak^{-\alpha_z}$, where k is wavenumber, and the spectral slope $-\alpha_z \sim \log\big(G_{z'}(k)\big)/\log(k)$. Values of -$\alpha_z$ for coral reefs range from -0.76 to -3.0 (Table 1). In this study, wavenumber spectra of the elevations about the mean bottom planform and their bottom slopes are calculated to quantify the roughness variability of rocky bottoms over horizontal length scales in both the alongshore and cross-shore directions.

High-resolution bathymetric surveys of complex bottoms are required to appropriately describe the roughness scales. High-resolution bathymetric surveys remain a costly, arduous task and often limit surveys to small, O(100mx100m) regions. In coral reef studies, multiple methods of obtaining high-resolution bathymetric surveys, O(cm), are used, including airborne topographic lidar, three-dimensional scanning multibeam sonar, unmanned aerial vehicle quadcopters, and autonomous underwater vehicles equipped with sidescan sonar (Table 1: Jaramillo and Pawlak, 2011; Rogers et al., 2019; Duvall et al.,2019, 2020). Evaluating the roughness of rocky bottoms along the length of California is uniquely possible owing to high-resolution (1-2m), nearshore seafloor datasets made available through the California Seafloor Mapping Program (CSMP) and the Seafloor Mapping Laboratory (SFML) at California State University Monterey Bay (CSUMB). The CSMP was formed to create coastal marine geological and habitat base maps for California's waters from Mean Higher High Water (MHHW) out to ~ 6km (Johnson et al., 2017). A total of 280 subaqueous (>5m water depth) bathymetric surveys were provided spanning California's ~1350km coastline. The California coast is complex owing to tectonics and geology. About 72% of the California coastline consists of rocky shores (Griggs et al., 2005), consistent with Bird's (2011) analysis that 75% of the world's shores are rocky.

Here, the subaqueous bottom roughness for rougher, rocky reefs along California is evaluated using CSUMB bathymetry. The research focuses on the intermediate scale. The methods for the preparation of the bathymetric surveys for analysis are described next in Chapter II, with the finding that rocky bottoms vary widely in appearance with no apparent typical bottom identified. In Chapter III, statistical analysis and results are presented and discussed in Chapter IV. The summary and conclusions are given in Chapter V, with a surprising conclusion that all the rocky bottoms examined are statistically similar and isotropic in cross-shore and alongshore in the range of intermediate wave scales (<666m).

II. METHODS-DATA PREPARATION

A. HIGH-RESOLUTION BATHYMETRY

Bathymetric surveys conducted from 2000-2014 were provided by the Sea Floor Mapping Laboratory (SFML) at California State University at Monterey Bay (CSUMB). The SFML used REASON Seabat multibeam sonars 8101, 8111, 7125, and 7111, with the model determined by the depth range of the survey area, and most having resolutions of ±20cm in the vertical and ±2m in the horizontal depending on the depth. SEA SWATHplus interferometric sidescan bathymetric sonars augmented the REASON multibeam systems in the extreme shallows (0-10m) (CSUMB-SFML, 2016). The inertial navigation system and global positioning system (GPS) that provided position and attitude had position accuracies of ± 2m in pitch and roll, heading accuracy of ±0.02°, and heave accuracy of ± 5cm. (CSUMB-SFML, 2016). Each survey varies in cross-shore and alongshore extent. The bathymetric data are described in meters in Universal Transverse Mercator (UTM, zones 10 and 11) Easting, Northing, and vertical elevations in MLLW.

Out of the 280 surveys, 102 surveys supported a spatial resolution of 1m or 2m that is adequate for describing the intermediate-scale, O(1-1000m), rocky morphology. The locations of the high-resolution surveys are shown in Figure 1. Excluded from the analysis herein are surveys with a spatial resolution coarser than 2m, those associated with bays and estuaries, and in locations where the bathymetry is altered by artificial structures (i.e., jetties and seawalls). Some regions were surveyed more than once, and the survey with the highest resolution with the most prominent coverage was selected. Lastly, surveys that did not extend to the 30m isobath were excluded.

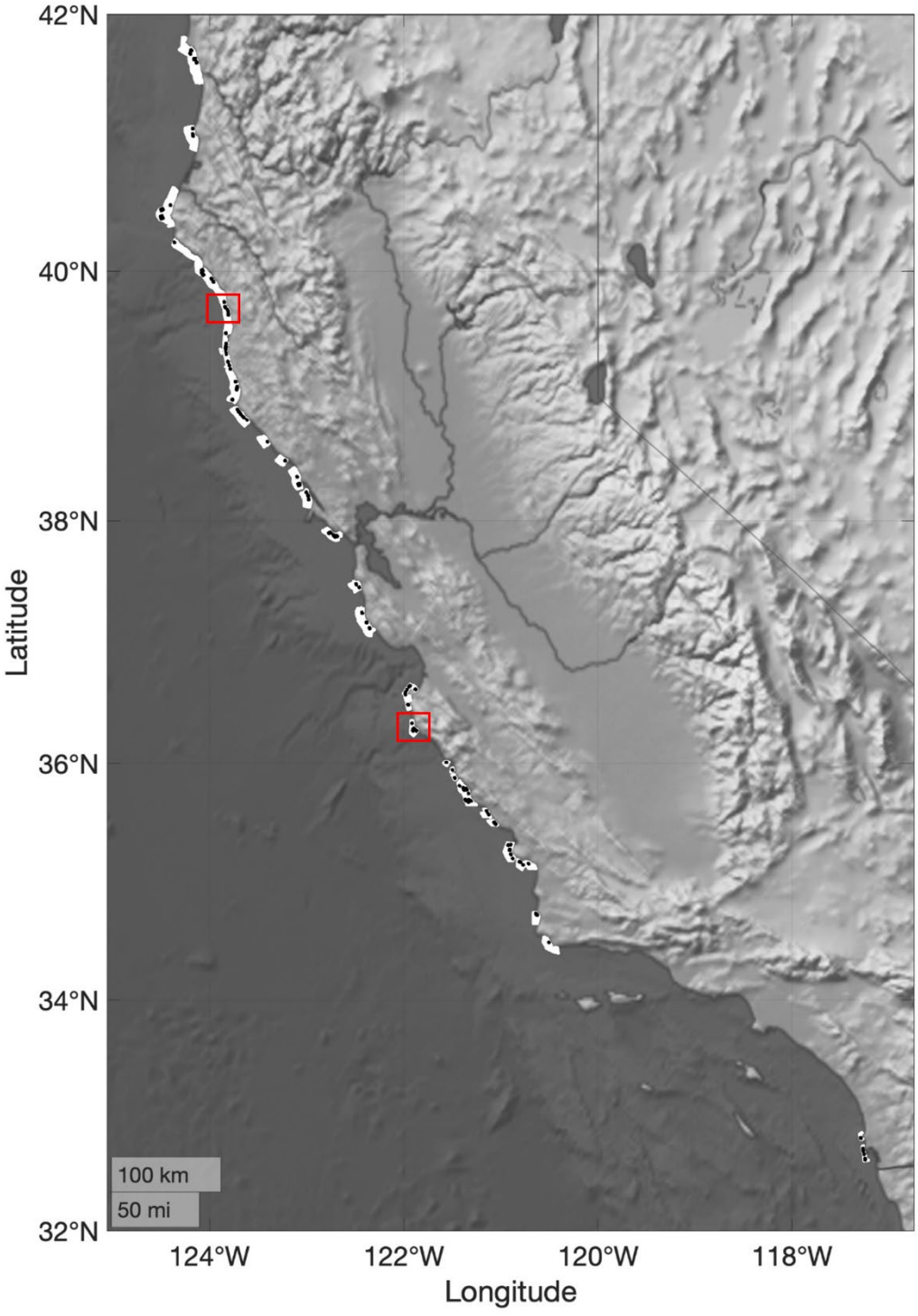

The high (1m and 2m) resolution bathymetric survey regions are denoted by white-filled polygons overlaid on a bathymetric and topographic map of California. Regions subjectively identified as rocky are denoted by black-filled polygons. The red boxes indicate the regions with the highest rocky bottom roughness.

Figure 1. Locations of bathymetry and rocky bottom subsets

B. INTERMEDIATE-SCALE, O(10-1000M), MORPHOLOGY

1. Local Coordinate Frame Transformation

Bathymetric surveys are transformed from a UTM geographic coordinate frame into a local coordinate frame for describing cross-shore (x) and alongshore (y). For a cross-shore and alongshore coordinate frame, a local (0,0) and rotation angle are required. The 30m isobath is the most consistent isobath amongst the bathymetric surveys and is the basis for describing the local coordinate frame. The Eastings and Northings (e_{30}, n_{30}) associated with the 30m isobath are extracted from the bathymetric data, where the subscript 30 represents the 30m isobath. The local (0,0) is the mean e_{30} and n_{30}. The rotation angle (θ_{30}) is determined by Principal Component Analysis (PCA) (Thomson and Emery, 2014) applied to e_{30} and n_{30}. The PCA major axis represents the alongshore direction, and the PCA minor axis represents the cross-shore direction (Figure 2). Depending on the orientation, the PCA analysis may have a180-degree ambiguity. To address the orientation ambiguity, the e and n are extracted for 27m and 33m isobaths using the same local (0,0) and are locally rotated by θ_{30}. The rotation is correct if x for the 33m isobath is located farther than the x for the 27m isobath. A 180-degree angle is added to the rotation angle if the opposite occurs. This procedure locally transforms all surveys. The assumption is that the rotated coordinate frame by the 30m isobath is the most representative of the cross-shore and alongshore orientations (Figure 2). This assumption matches the relative shoreline orientation for straight coastlines. Here the PCA major axis is much greater than the minor axis. For surveys associated with strongly curved or abrupt coastlines (e.g., regions around the Monterey Peninsula, Figure 2), the assumption is no longer valid, as seen by an increase in the PCA minor axis relative to the major axis. The procedure is still applied for complex shorelines. The orientations of intermediate-scale statistics are evaluated to determine the validity of using the 30m isobath to define the local coordinate frame.

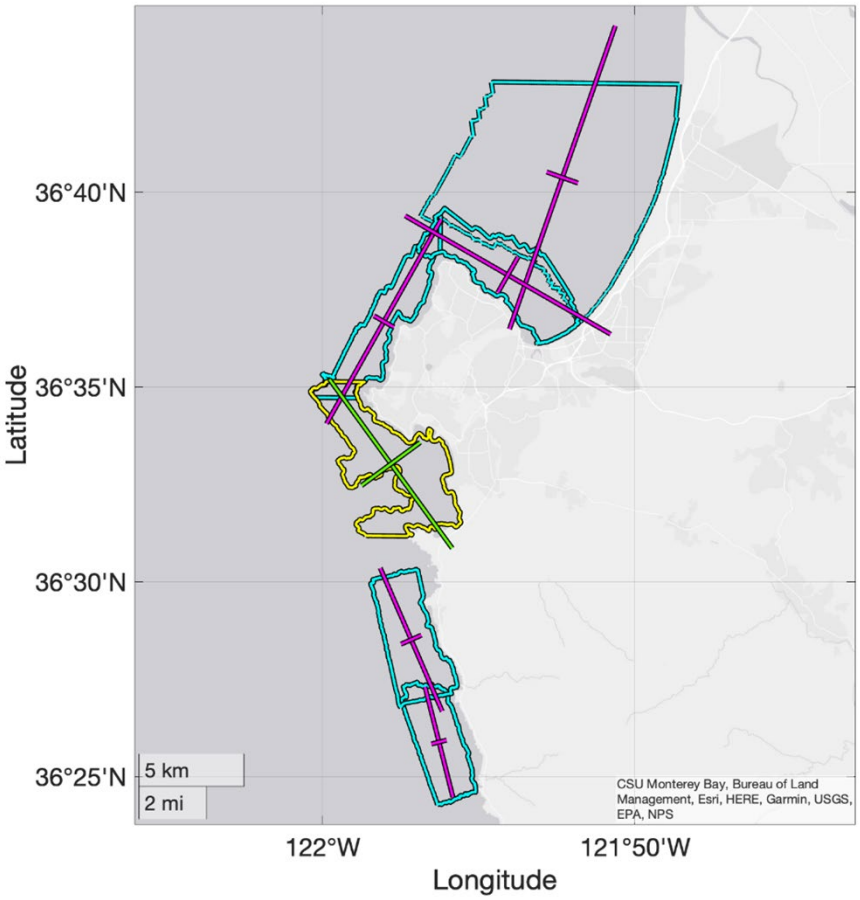

Examples of the local coordinate frame transformation for varying bathymetric surveys (outlined in cyan and yellow) around the Monterey Peninsula based on the PCA of the e_{30} and n_{30}. The magenta lines represent the PCA major (alongshore), and minor (cross-shore) axes associated with e_{30} and n_{30}. The survey outlined in yellow with green PCA major and minor axes is an example that occurs along a strongly curved coastline.

Figure 2. Monterey Peninsula Principal Component Analysis (PCA)

2. Intermediate-Scale Bathymetry

The intermediate-scale bathymetry is separated from the total bathymetry (Figure 3a) defined in the locally rotated coordinate frame. First, a low-pass filter described by a running average is applied to the bathymetric surveys to describe the large-scale bathymetry. The average of z is computed with a 750m-square window and spatially defined at the center of the window. The window is spatially shifted by 75m in both the cross-shore and alongshore directions across the survey (Figure 3a). The running spatial average represents the large-scale bathymetry (Figure 3b). A window size of 750m was

chosen, as it represents the approximate wavenumber cutoff between shoaling wave processes and those associated with Bragg scattering and bottom friction (Ardhuin et al., 2003). The intermediate-scale results were similar using the 75m spatial step to that of the resolution (e.g., 1m or 2m) though computationally more efficient. The running average has inherent edge effects, which are accounted for by a spatial coverage percentage. The percentage of spatial coverage is defined as the available observations divided by the total amount within a 750m-square window multiplied by 100 (Figure 3c). A reduction in spatial coverage occurs near the edges. Here the spatial extent is limited to spatial coverages greater than 60% (green line in Figure 3a,c). The 75m-spaced, large-scale bathymetry is linearly interpolated to the original 1m or 2m resolution. The surface elevation (z') of the intermediate-scale bathymetry (Figure 3d) is computed by subtracting the large-scale bathymetry (mean planform) (Figure 3b) from the total bathymetry (Figure 3a).

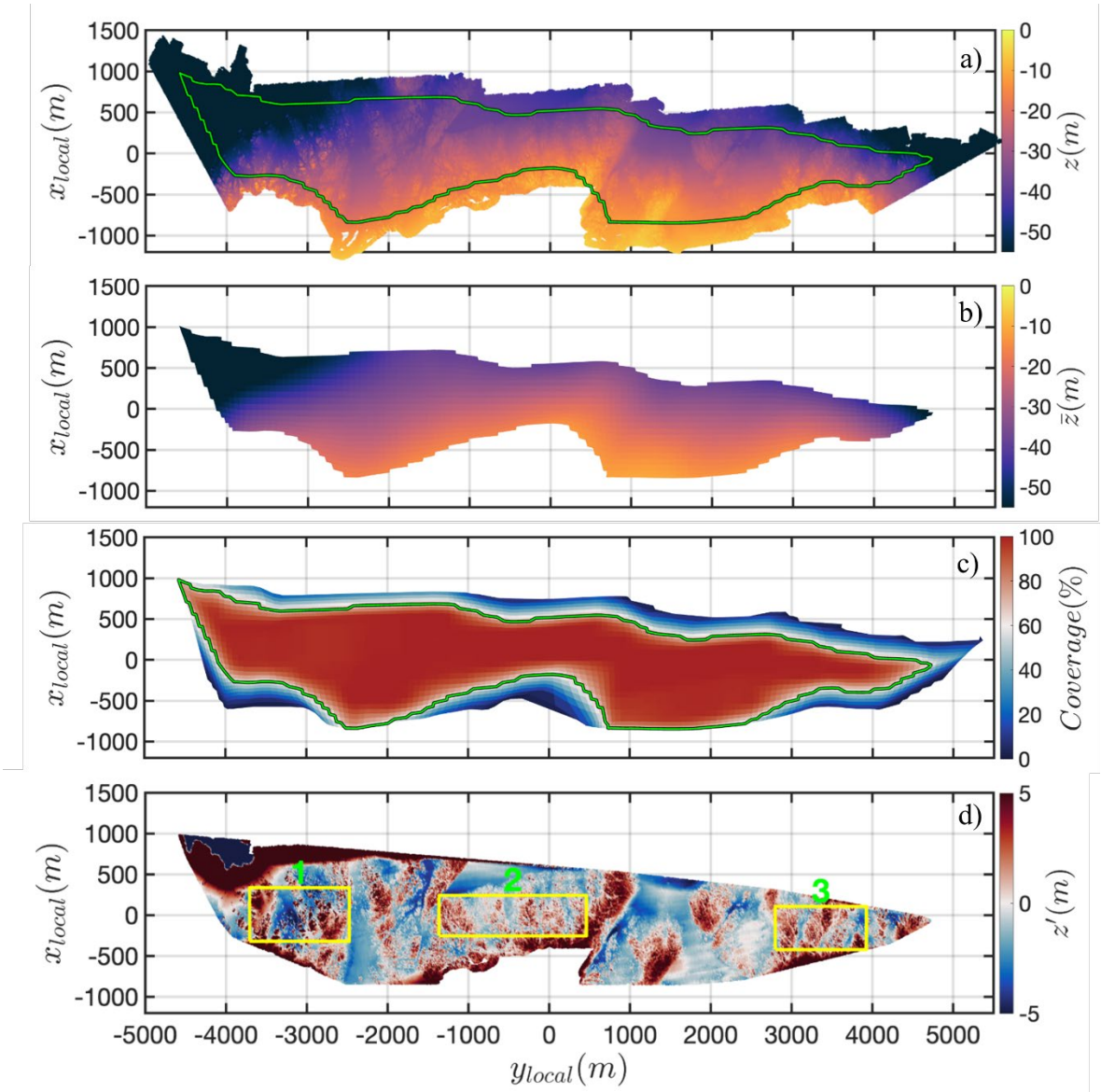

a) The total bathymetric survey from Cypress Point to Point Pinos off the Monterey Peninsula, defined in a local, rotated coordinate frame. b) The large-scale bathymetry computed spatially using a running mean average with a 750m-square window. c) The percentage of spatial coverage that occurs within the 750m-square boxes. d) The surface elevation (z') of intermediate-scale bathymetry obtained by subtracting the large-scale averaged bathymetry from the total survey. The yellow boxes represent the rocky bottom subsets that are visually selected for analysis. The green lines denote the location where the spatial coverage is 60%.

Figure 3. Bathymetry of Cypress Point to Point Pinos, Monterey Peninsula

3. Selecting Representative Rocky Bottoms

Rocky bottom subsets were visually selected from intermediate-scale bathymetric maps to represent rocky bottoms. Rocky shores are complex and are often described by irregular mixed sections of sandy shores and rocky shores. The complexity of including mixtures of rock and sand bottoms is outside of the focus of the study herein but requires a subjective selection of rocky bottom subsets. There can be multiple subsets in a bathymetric survey. Examples of rocky bottoms selected for heterogeneity are outlined in yellow boxes in Figure 3d. The selection is based on areas that appear rocky and are nearly continuous in being rocky for approximately 1000m in the alongshore and 500m in the cross-shore. The alongshore distances range from 800m to 3300m, averaging 1345m. The cross-shore lengths range from 200m to 2400m, with an average of 860m. The rocky bottom subsets selected are compared against available USGS seafloor compositional maps to verify that the subset co-occurs with rocky seafloor composition (Golden, 2016). A total of 99 rocky bottom subsets were selected believed to be representative rocky bottoms along the length of California (Figure 1, black polygon regions). Of the 99 rocky bottoms, 11 have 1m resolution and 88 have 2m resolution. Inspection of all 99 rocky bottoms finds a wide variety of planforms with no "typical rocky bottom" identified. The yellow box 2 (Figure 3d) is selected as an example of rocky bottom elevations for closer examination. Once the subset is selected, the bottom slopes in the alongshore and cross-shore are calculated (Figures 4b,c). The bottom slopes are calculated by taking the difference in the z' divided by the resolution of the survey. In the rocky bottom of Figure 4a, the rocks appear to be slightly oriented in the cross-shore. For the bottom slopes, however, it is hard to identify an orientation and to discriminate the differences between x and y bottom slopes.

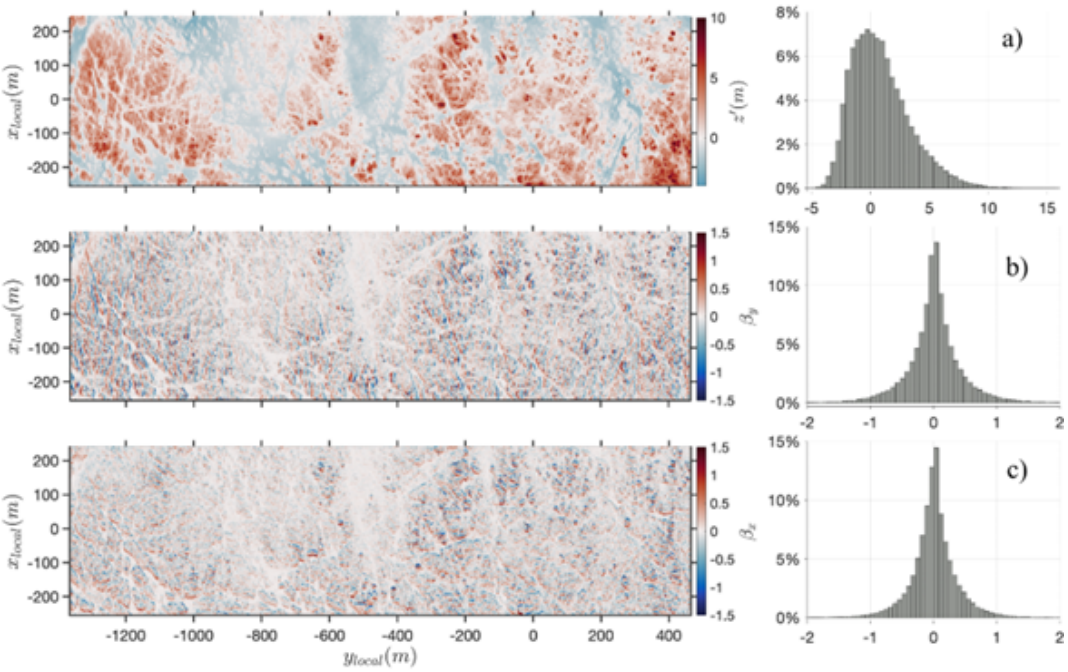

a) Example of an expanded view of the rocky bottom subset for bathymetry in the vicinity of China Rock (Figure 3d yellow box 2) and histogram of bottom elevations, z'. b) Bottom slope in the alongshore (βy) and histogram of βy. c) Bottom slope in the cross-shore (βx) and histogram of βx.

Figure 4. Rocky bottom slopes in the alongshore and cross-shore directions

III. RESULTS

The roughness as measured by the standard deviations of z' ($\sigma_{z'}$) and slope (σ_β) are plotted by latitude for each rocky bottom survey (Figures 5a,b). The σ_β are calculated as the mean value of all slopes in the x- and y-directions for each subset. The $\sigma_{z'}$ range from 0.35m to 8.6m with a mean of 2.1m. The σ_β range from 0.01 to 0.81 with a mean of 0.22. There is an apparent correlation between bottom variability and bottom slope. Histograms for $\sigma_{z'}$ and σ_β are shown beneath in Figures 5c and 5d.

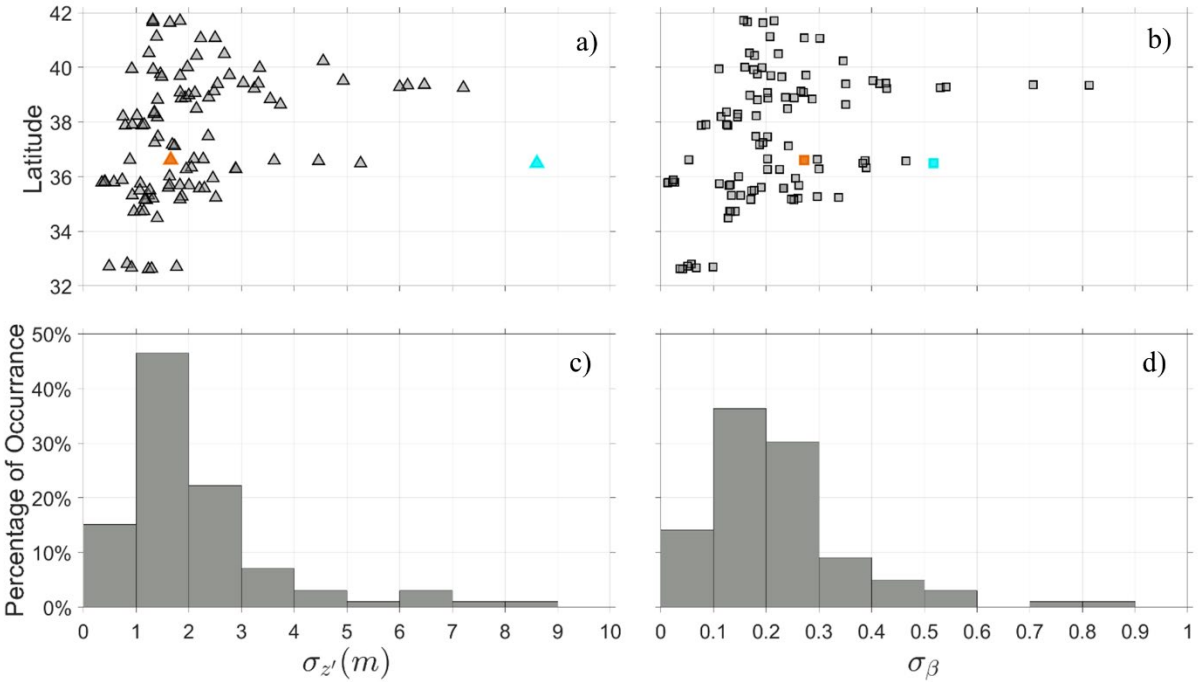

a) Standard deviations of z' (triangles) for all 99 rocky bottom surveys shown in Figure 1 by latitude. b) Standard deviations of β (squares) for all rocky bottom surveys shown in Figure 1 by latitude. c) Histogram of $\sigma_{z'}$ and d) histogram of σ_β. The orange triangle and square correspond to China Rock (Figure 4), and the blue triangle and square correspond to Yankee Point (Figure 11).

Figure 5. Standard deviations of z' and β by latitude and histograms of $\sigma_{z'}$ and σ_β

Linear regression analysis is performed to evaluate the relation between σ_β and $\sigma_{z'}$ shown in Figures 5 a,b. A mean slope of 0.08 with a value of R^2=0.75 is calculated (Figure 6).

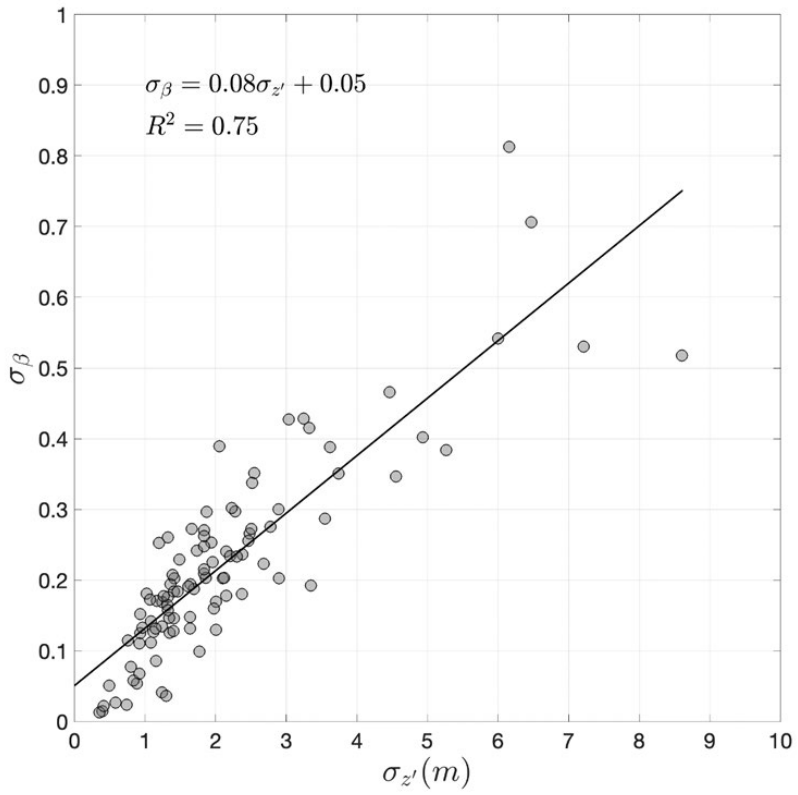

Figure 6. Linear regression of σ_β with $\sigma_{z'}$

Probability density functions (pdf) of $\widehat{z'}$, $\hat{\beta}_x$, and $\hat{\beta}_y$ (hats indicate transformed to a standard normal variable) along with standard deviation, mean, skewness, and kurtosis calculated for all 99 rocky bottom subsets. Examples of the pdfs for the subset in Figure 4 (China Rock) and the subset with the largest standard deviation of z' (Yankee Pt.) are shown in Figure 7. The mean statistics for all 99 rocky bottom subsets and four example rocky bottom subsets are given in Table 2.

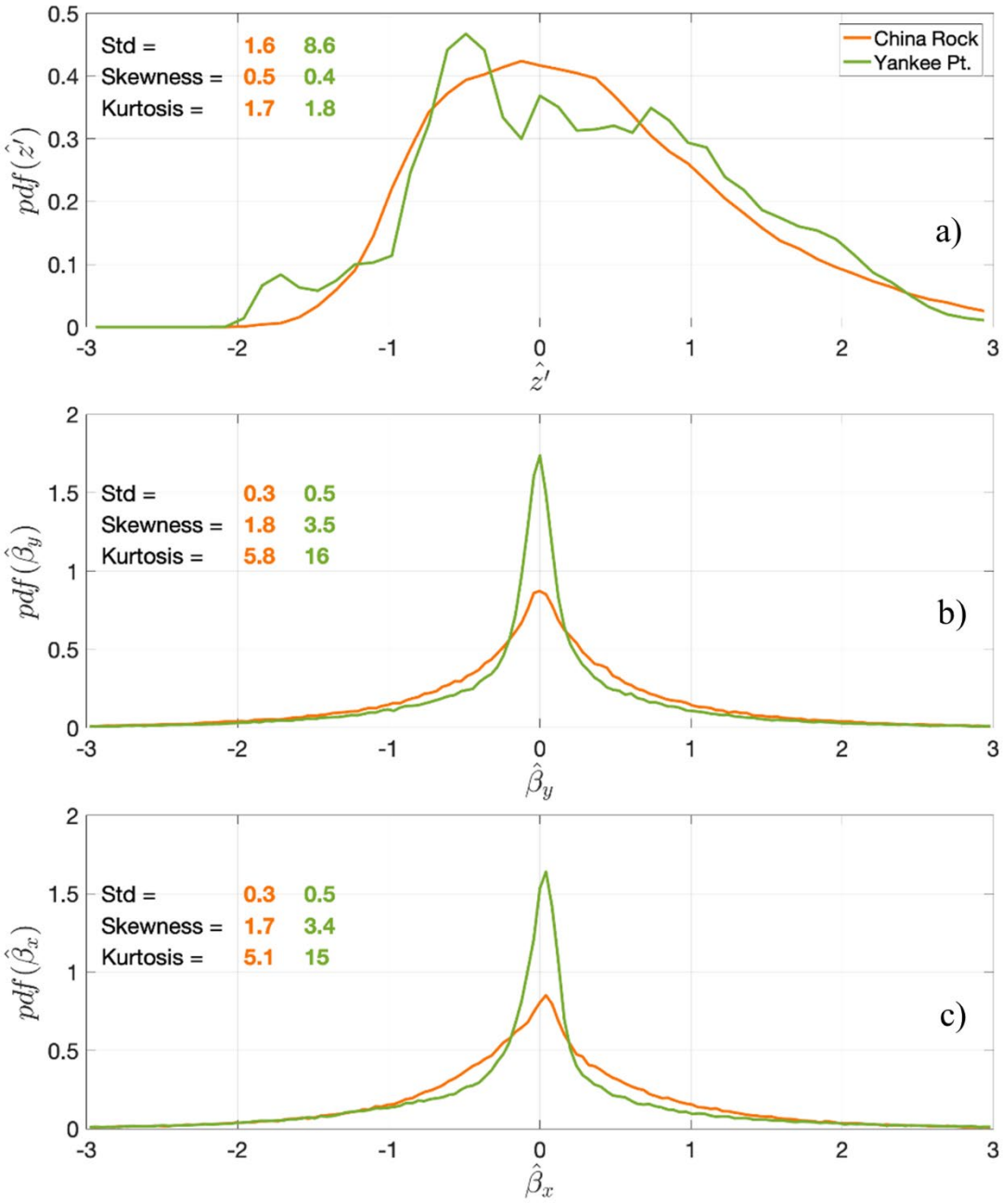

Examples of probability density functions for the subset in Figure 4 (China Rock) and the subset with the largest standard deviation (Yankee Pt.): a) Elevation pdf($\widehat{z'}$). b) Alongshore (x-direction) rocky bottom slope pdf($\hat{\beta}_x$). c) Cross-shore (y-direction) rocky bottom slope pdf($\hat{\beta}_y$). Hats indicate using a standard normal variable.

Figure 7. Distributions of z' and bottom slopes

Table 2. Rocky bottom statistics

	All 99 subsets	CyPt to PtPn (1)	CyPt to PtPn (2) (China Rock)	CyPt to PtPn (3)	Yankee Point
$\sigma_{z'}$ (m)	2.1	3.6	1.6	2.2	8.6
$\sigma_{\beta x}$	.22	.37	.25	.29	.53
$\sigma_{\beta y}$	.22	.40	.29	.31	.51
$S_{z'}$	.80	.49	.48	.59	.43
$S_{\beta x}$	2.9	3.1	1.7	1.7	3.4
$S_{\beta y}$	3.0	3.0	1.8	1.7	3.5
$K_{z'}$	2.6	1.7	1.7	1.8	1.8
$K_{\beta x}$	14	13	5.1	5.3	15
$K_{\beta y}$	15	12	5.8	5.1	16

The standard deviation (σ), skewness (S), and kurtosis(K) of z', βx, and βy. Column two lists the statistics for all 99 rocky bottom subsets. Columns three through five show statistics for Cypress Point (CyPt) to Point Pinos (PtPn) and rocky bottom subsets 1, 2, and 3 (Figure 3d). Column six is the statistics for Yankee Point (Figure 11).

For determining roughness with length scales, wavenumber spectra are calculated for z', $\widehat{G_{zz}}(k)$, and bottom slopes β, $\widehat{G_{\beta\beta}}(k)$, in both the x- and y- directions every 1m or 2m dependent on the resolution for each rocky bottom subset. The hat signifies ensemble averaging. Individual wavenumber spectra of z' in the x-direction, $G_{zz}(k)$, are calculated for each cross-shore profile for every increment in the alongshore direction about the mean planform (e.g., Figure 4a) by detrending the profile, applying a Hanning window, and normalizing by dividing by the high-passed variance (>1/750m). The ensemble-averaged normalized spectrum of z' in the x direction, $\widehat{G_{zz}}(k)$, is then calculated as the average of all the cross-shore spectra. The degrees of freedom are two times the number of cross-shore profiles, nominally 1345 degrees of freedom for the 2m resolution data. A similar procedure is performed for z' in the y-direction resulting in a normalized ensemble average spectrum with nominally 860 degrees of freedom for the 2m resolution data. All 99 rocky bottom $\widehat{G_{zz}}(k)$ for x and y are shown in Figure 8a. The $\widehat{G_{zz}}(k)$ in x and y are similar in shape and approximately isotropic. The result is that the cross-shore and alongshore spectra are plotted together over each other as $\widehat{G_{zz}}(k)$ (Figure 8a). The

variance of $\widehat{G_{zz}}(k)$ is dominant at low wavenumbers and decreases towards the highest wavenumbers by two orders of magnitude. There is apparent higher variability of the spectra at the higher wavenumbers that may result from normalizing by the total variance, where the total variance is dominated at low wavenumbers. The curve up at the highest wavenumbers is owing to aliasing about the Nyquist wavenumber. The spectra appear to have at least two power law slopes, which are examined next.

The slopes of the log$G_{zz}(k)$ spectra, $log\ \alpha_z = d(logG_{zz}(k))\ /\ (d(log\ (k)\ )$, are calculated by computing a linear regression for five successive spectral estimates moving one k interval at a time across each $logG_{zz}(k)$ for all 99 rocky bottom subsets for both x and then y directions. Then the slopes from all rocky bottom spectra are binned into forty equal logarithmically spaced bins to obtain a mean ensemble averaged slope, $\widehat{\alpha_z}(k)$, for both x and y (Figure 8c). The $\widehat{\alpha_z}(k)$ gradually decrease with wavenumber from -1 to -3. The turn-up at high wavenumbers owing to aliasing is even more pronounced as differentiating the spectrum (calculating the slope) acts like a high pass filter that accentuates high wavenumbers. The spectra in Figures 8c,d have been truncated at the Nyquist for the 2m resolution data. The 95% confidence intervals are computed for each bin based on the degrees of freedom for 99 averaged values times the number of spectral estimates in each bin times two that vary across the spectrum. The x and y slope spectra are similar except at low wavenumbers. The confidence intervals of x and y spectra overlap for wave numbers >(1/666m), indicating the $\widehat{\alpha_z}(k)$ are isotropic within this region of wavenumbers with 95% confidence.

The bottom slopes of z's in x and y are computed as a measure of roughness by calculating the difference between adjacent points and dividing by the respective resolution (e.g., Figures 4b,c). The wavenumber spectra for bottom slopes, $\widehat{G_{\beta\beta}}(k)$, in x and y are calculated in the same manner used to calculate the $\widehat{G_{zz}}(k)$ by detrending the data, applying a Hanning window, and normalizing by dividing by the high-passed variance (>1/750m) and ensemble-averaging. The normalized spectra for bottom slopes in x and y are also similar and are therefore plotted over each other as $\widehat{G_{\beta\beta}}(k)$ (Figure 8b). The variance of $\widehat{G_{\beta\beta}}(k)$ is dominant at a middle wavenumber of about 0.05 m^{-1}

(1/25m). The curve up at the highest wavenumbers is again owing to aliasing about the Nyquist wavenumber.

The spectral slopes for the bottom slope wavenumber spectra, $\widehat{\alpha_\beta}(k) = d(log(\widehat{G_{\beta\beta}}(k))/d(\log(k))$, are calculated in the same manner as $\widehat{\alpha_z}(k)$ above for all 99 rocky bottom subsets for both x and y directions. (Figure 8d). The slopes of the bottom slope spectra are statistically isotropic over wavenumbers >1/666m based on the overlapping confidence intervals between the x and y slope spectra. The $\widehat{\alpha_\beta}(k)$ decrease with wavenumber from .75 to -1.5 and have shapes similar to the $\widehat{\alpha_z}(k)$ (compare Figure 8d with 8c and note different scales). The turn-up at the highest wavenumbers again is owing to aliasing.

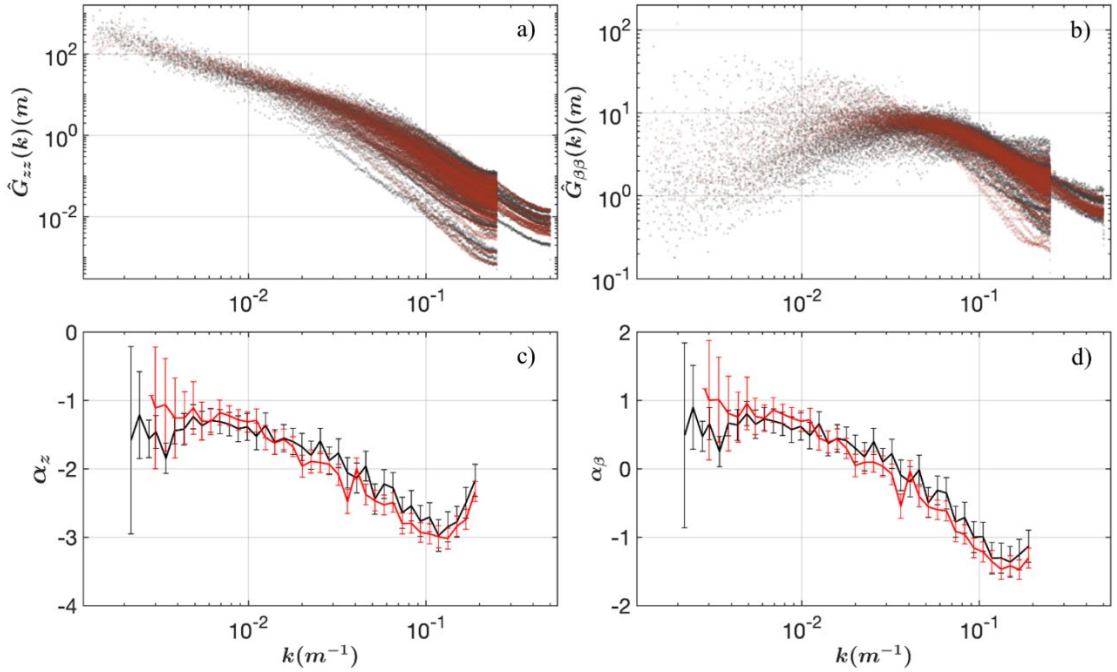

99 rocky bottom wavenumber spectra: a) Normalized (by variance) wavenumber spectra of z', $\widehat{G_{zz}}(k)$. b) Normalized (by variance) wavenumber spectra of bottom slopes, $\widehat{G_{\beta\beta}}(k)$. c) Averaged $\widehat{G_{zz}}(k)$ spectral slopes ($\alpha_{z'}$). d) Averaged $\widehat{G_{\beta\beta}}(k)$ spectral slopes (α_β). Black lines are the y-direction (alongshore), and red lines are the x-direction (cross-shore). The vertical black and red lines are the 95% confidence intervals.

Figure 8. Average spectra and spectral slopes of z' and bottom slope of rocky bottoms

Standard deviations of z' in the x and y directions are calculated as the area under the high-pass spectra of z'. A high-pass cutoff of 1/666m is used because if the cutoff of 1/750m is used the standard deviations are dominated by variance at lowest wavenumbers, where the spectral slopes in x and y diverge at 1/666m (see Figure 8c,d). The histogram of the standard deviations of z' in the x-direction divided by the y-direction is shown in Figure 9a. 80% of the ratios occur within ±20% of 1, suggesting the rocky bottoms are approximately isotropic in the x- and y-directions. The histograms of the standard deviations of the bottom slopes in the x-direction divided by the y-direction are shown in Figure 9b. 87% of the ratios occur within ±20% of 1, also suggesting the rocky bottoms are approximately isotropic in the x- and y-directions.

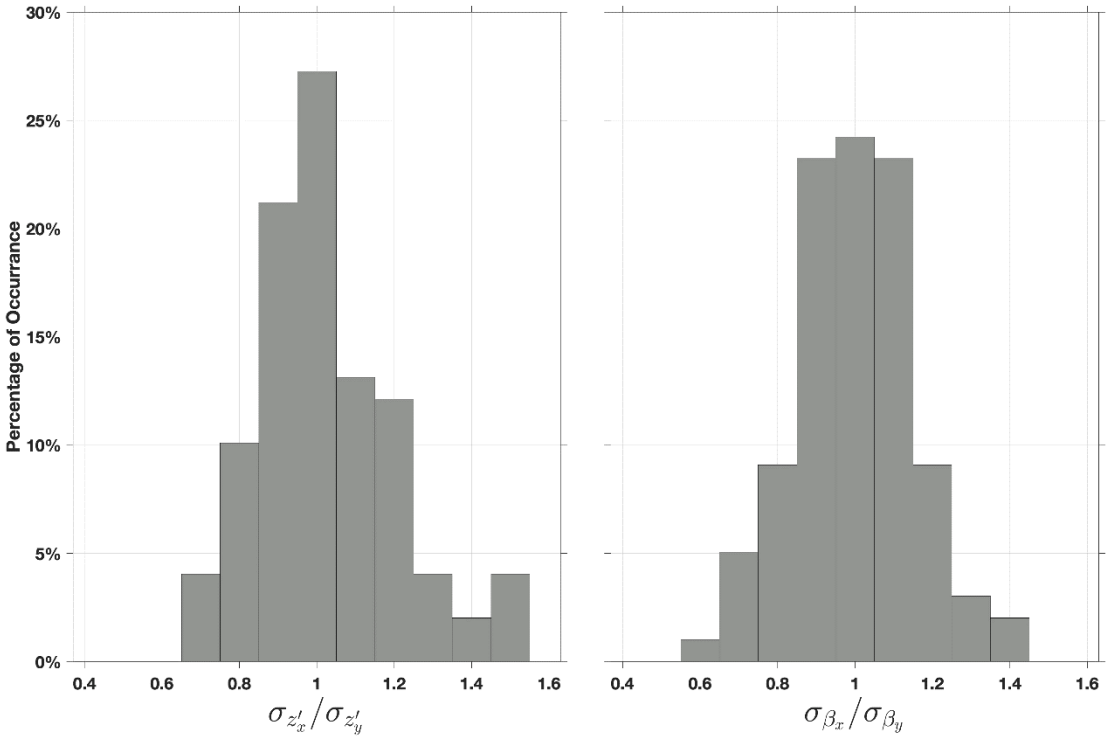

a) Ratio of the standard deviations of z' in the x-direction (cross-shore) divided by the y-direction (alongshore). b) Ratio of the standard deviation of the bottom slopes in the x-direction (cross-shore) divided by the y-direction (alongshore).

Figure 9. Histogram of the ratio of the standard deviations in x- and y-directions

THIS PAGE INTENTIONALLY LEFT BLANK

IV. DISCUSSION

A. BOTTOM ROUGHNESS

The roughness of the bottom is measured as the standard deviation of the elevation (z') about the demeaned planform, $\sigma_{z'}$, for the ninety-nine selected rocky bottoms along the California Coast (Figure 5a). The largest $\sigma_{z'}$ are located approximately at latitudes of 36.5N and 39.2N. The mean $\sigma_{z'}$ for all subsets is 2.1m with a range of 0.35 to 8.6. By comparison, coral reef $\sigma_{z'}$ ranged from 0.03 to 0.99m. The rocky bottom at China Rock (Figure 4), for which $\sigma_{z'}$= 1.7m, has large undulations spread out over the 1800m by 500m subset with peaks (red) up to 10m, and relatively large areas of flat depressions (-2m) displayed in blue. For comparison, the rocky bottom with the largest $\sigma_{z'}$ out of the ninety-nine rocky bottom subsets is 8.6m at Yankee Point (Figure 10). The bottom at Yankee Point has large undulations spread out over the 1100m by 600m subset with peaks (red) up to 35m, and relatively large flat depressions (-15m) displayed in blue.

The bottom slopes of the rocky bottom subsets are calculated as another measure of roughness. The standard deviations of bottom slope, σ_β, are found to be largest at the same locations that have the highest $\sigma_{z'}$ (Figure 5b). Qualitatively, it is difficult to distinguish by eye the differences between plan views of the slopes in x and y shown in Figures 4b,c, and 10b,c. The areas with a larger positive or negative slope in the x direction are similar to areas with a larger positive or negative slope in the y direction. The white areas representing 0 slope are in the same areas in both x and y and generally occur in depressions indicated by negative z' (blue). The depressions presumably are filled with sediments that are relatively smooth. To quantify the suggested isotropy, the distribution of the ratio of $\sigma_{z'}$ in the x-direction are divided by the $\sigma_{z'}$ in the y-direction are calculated. 80% of the ratios are found to occur within $\pm$20% of 1 (Figure 8a). The ratios for σ_β are similarly calculated with 86% of the ratios occurring within $\pm$20% of 1 (Figure 8b), indicating the rocky bottoms are approximately isotropic in the x- and y-directions.

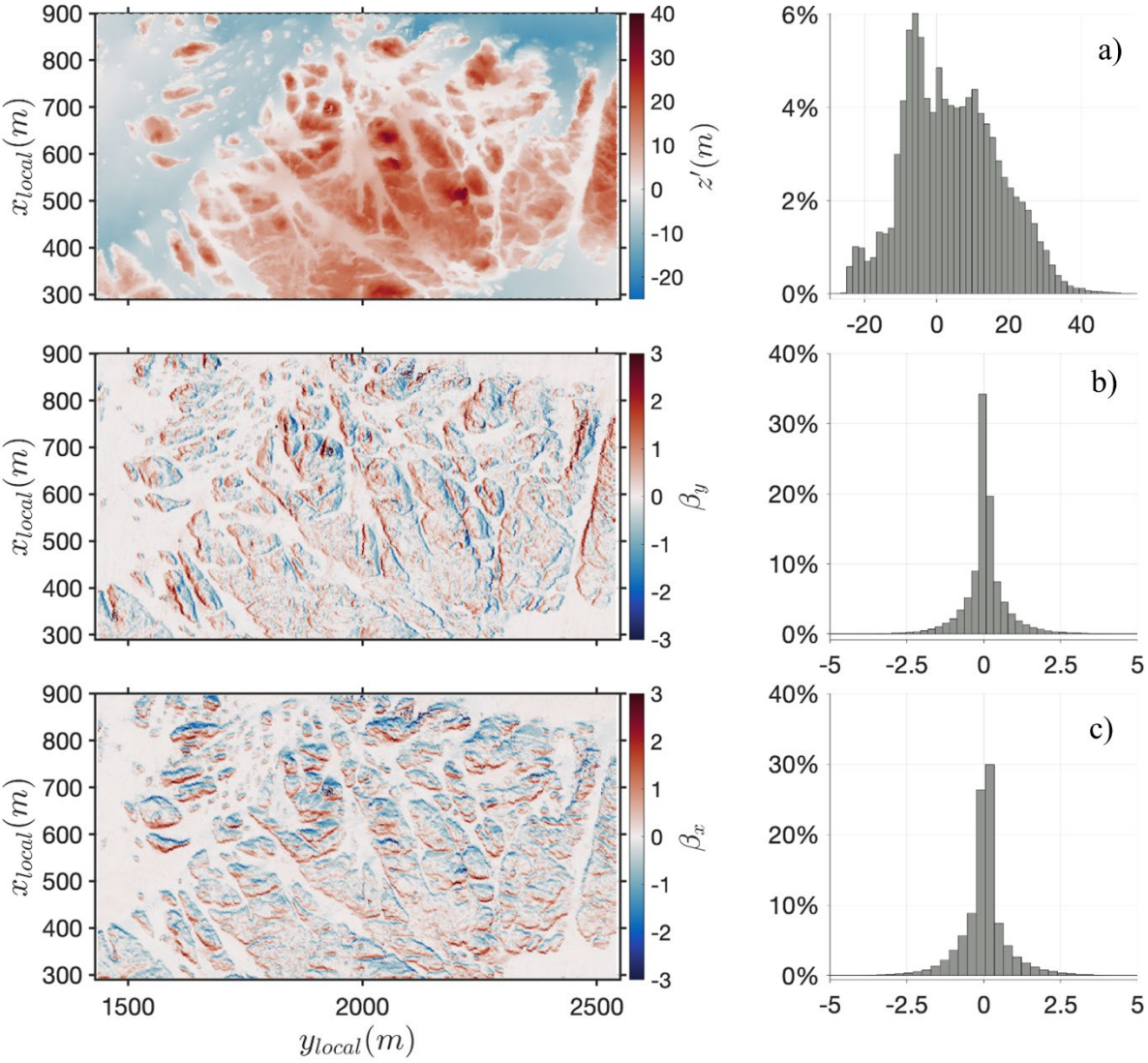

a) The rocky bottom subset with the largest $\sigma_{z'}$=8.6m at Yankee Point bathymetry. b) Bottom slope in the alongshore (β_y) of the rocky bottom subset. c) Bottom slope in the cross-shore (β_x).

Figure 10. Rocky bottom elevation (z') and bottom slopes (β) of Yankee Point

B. WAVENUMBER SPECTRA OF Z'

The wavenumber spectra of z' and their spectral slope spectra are computed as a measure of roughness with scale. The ensemble-averaged normalized wavenumber spectra of elevations $\widehat{G_{zz}}(k)$ in x and y for all 99 rocky bottom subsets are similar across wave numbers (Figure 8a) as further evidence the rocky bottoms are near isotropic and homogeneous in x and y. The three coral sites studied by Duvall, et al. (2020) also

exhibited isotropy. However, the coral reefs were over separate inhomogeneous areas. On the other hand, sandy bottoms tend to be homogeneous but may be strongly anisotropic owing to directional sand features such as linear ripples (Jackson and Richardson, 2007) or large sand ridges up to 10m heights found by Ardhuin et.al. (2003). The wave-number elevation spectra are limited to intermediate wave process scales of <750m, which does not capture all of the variance as $\widehat{G_{zz}}(k)$ are still increasing at the lowest wavenumbers (<1/750m). Thus, the variance along the California coast is calculated at limited scales. The spectra are red with the spectral density highest at the largest scale features and decreasing for the smaller-scaled features (Figure 8a), which was also found by coral reef researchers (Table 1). It was found in the previous coral reef studies that wavenumber spectra could be described in terms of a constant power law where the $logG_{zz}(k)$ spectra had a constant slope in *log k*. The spectral slopes of z' of coral reefs ranged from -.76 to -3.0 (Table 1). The averaged wavenumber spectra of the spectral slopes $\widehat{\alpha_z}(k)$ for all 99 rocky bottom subsets in x and y are isotropic with 95% confidence for *k*<1/666m (Figure 8c). The x spectral slopes at wavenumbers lower than 1/666m tend to flatten or decrease, whereas the spectral slopes in y tend to increase. The $\widehat{\alpha_z}(k)$ range from -1.0 to -3.0, proceeding from lowest to highest wavenumbers (Figure 8c).

C. BOTTOM SLOPE WAVENUMBER SPECTRA

The bottom slope ensemble-averaged normalized wavenumber spectra, $\widehat{G_{\beta\beta}}(k)$, and their averaged slopes, $\widehat{\alpha_\beta}(k)$, in x and y are calculated for the rocky bottom subsets (Figures 8 b,d). The spectral slopes $\widehat{\alpha_\beta}(k)$ range from 1 to -1 (Figure 8d). The averaged slope spectra for surface elevation $log\ \widehat{\alpha_z}(k)$ and the slope wavenumber spectra $log\ \widehat{\alpha_\beta}(k)$ are identical in shape with a shift of +2 in magnitude (compare Figures 8d with 8c). The $\widehat{\alpha_\beta}(k)$ are also isotropic.

Rogers et al. (2018) found in coral reef studies that finer resolved bathymetry resulted in greater variance in z'. They examined bottom slope spectra with varying resolutions from 6 to 270cm. The maxima of the spectra appeared to shift to lower wavenumbers as the resolution increased. Here, bottom slope spectra with different resolutions were examined by truncating the 1m resolution bottom data to 2m and 4m.

No difference in spectral shape could be discerned for different resolutions (not shown). Therefore, it is concluded that there is no significant difference in the spectra as the resolution increases, at least for the resolutions examined here.

D. FOURIER MODEL OF BOTTOM ROUGHNESS

Following Duval et.al. (2020), the rough bottom elevation in the x-direction can be represented in Fourier space as

$$z(x) = A(k)\sin(kx + \varepsilon) \quad [1]$$

where $A(k)$ is the amplitude of the Fourier component, and ε is a random phase. The wave-number spectrum is approximated as

$$G_{zz}(k) = \frac{A(k)^2}{2\Delta k} \quad [2]$$

The slope can be expressed as

$$\frac{dz}{dx} = A(k)\,k\cos(kx + \varepsilon) \quad [3]$$

The slope spectrum is similarly given by

$$G_{\beta\beta}(k) = \frac{k^2 A(k)^2}{2\Delta k} = k^2 G_{zz}(k) \quad [4]$$

Building on these results and letting the normalized wave number spectrum be given by a power law

$$G_{zz}(k) = B(k)\,k^{-\beta(k)} \quad [5]$$

where $B(k)$ is the spectral magnitude, $\beta(k)$ is a local slope. Then,

$$\log G_{zz}(k) = \log B(k) - \beta(k)\log k \quad [6]$$

From [4] and [5], the slope spectrum is

$$G_{\beta\beta}(k) = k^2 B(k)\, k^{-\beta} = k^2 G_{zz}(k) \quad [7]$$

where k^2 acts as a transfer function transforming $G_{zz}(k)$ to $G_{\beta\beta}(k)$. Taking the log of [7] gives

$$\log G_{\beta\beta}(k) = \log B(k) + (2 - \beta(k)) \log k \quad [8]$$

The interest here is to relate the slope spectra of the bottom elevations to the bottom slopes. The slope spectra from [6] and [8] are given by

$$\frac{d\log G_{zz}(k)}{d\log k} = \frac{d\log(B(k))}{d\log k} - \beta(k) - \log(k)\frac{d\beta(k)}{d\log k} \quad [9]$$

and,

$$\frac{d\log G_{\beta\beta}(k)}{d\log k} = \frac{d\log(B(k))}{d\log k} + (2 - \beta(k)) - \log(k)\frac{d\beta(k)}{d\log k} \quad [10]$$

where here $\log\alpha_z(k) = \dfrac{\log G_{zz}(k)}{d\log k}$ and $\log\alpha_\beta(k) = \dfrac{\log G_{\beta\beta}(k)}{d\log k}$.

Combining [9] and [10],

$$\log\alpha_\beta(k) = \log\alpha_z(k) + 2 \quad [11]$$

The effect of applying the transfer in log space is to shift the spectral slopes of the z' spectra by a magnitude of +2, giving the same shape (dotted line) compared with the spectra of the bottom slope spectra (Figure 11). The spectral slopes of the surface elevation are all negative. However, shifting the magnitude by +2 results in the spectral slopes of the bottom slopes being positive and negative. The transformed bottom elevation spectra compare well with the spectra of the independent directly measured bottom slopes except at the lowest and highest wavenumbers (Figure 11). The differences between measured and transformed spectra at low numbers may be due to the noisiness (variability) of the bottom slope spectra at low wavenumbers or a bias in the transformed slopes owing to differentiating at the highest wave number (Brandt and Brincker, 2014).

The discrepancies at the highest wavenumbers are associated with the aliasing. When transforming $G_{zz}(k)$ to $G_{\beta\beta}(k)$ the 2 orders higher energy is transformed into the aliased tail, making it too large. It is found that using a Fourier representation of the bottom elevation gives a good representation of the bottom.

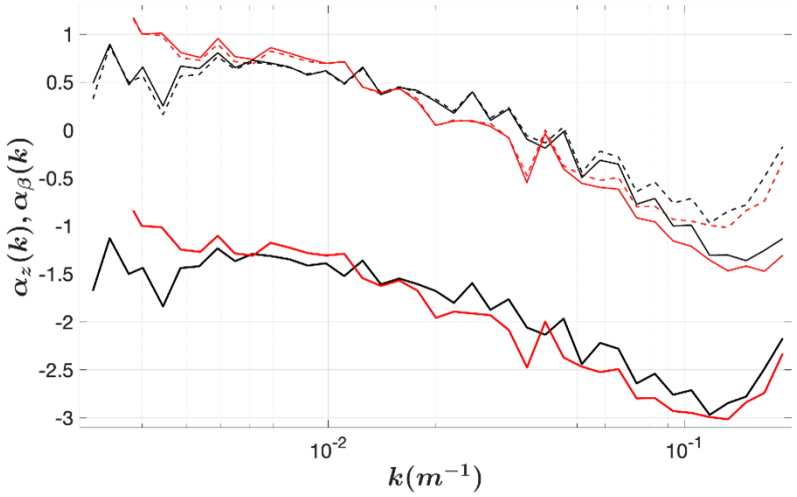

The lower black (x-direction) and red (y-direction) curves are spectral slopes for z' spectra, $\widehat{\alpha_z}(k)$ for the rocky sub boxes. The upper black (x-direction) and red (y-direction) curves are the spectral slopes of the bottom slope spectra, $\widehat{\alpha_\beta}(k)$. The dashed black and red lines are the result of applying the transfer function of the spectral slopes of z' (eq. 11).

Figure 11. Transfer function of the spectral slope

The $\widehat{G_{\beta\beta}}(k)$ tend to have maxima at intermediate wavenumbers (Figure 9b). Individual unnormalized $\widehat{G_{\beta\beta}}(k)$ are smoothed using a 5-point running average and the location of the maxima is determined (Figure 12). The maxima in $\widehat{G_{\beta\beta}}(k)$ indicate at what scale the bottom has the steepest slope. 80% of the maxima fall in the range of 15 to 80m. Rogers et al. (2018) concluded that for fully developed turbulent flow expected over rough coral reef bottoms, the bottom stress is dominated by form drag that is greatest for the steepest slope; they associated the steepest bottom slope at the maximum of $\widehat{G_{\beta\beta}}(k)$ as the scale of dominant hydrodynamic processes.

Ardhuin et al. (2003) calculated bottom slope wavenumber spectra for the sandy bottom shelf off Duck, North Carolina with regions of large sand ridges and ripples owing to wave motion indicated (Figure 12). The rocky bottoms measured here are orders of magnitude greater than the sandy bottom roughness over all scales. Regions of wave processes dominated by wave refraction and Bragg scattering are indicated. Using Ardhuin's scale, it is found that the bottom slope wavenumber spectra of the ninety-nine rocky bottom subsets occur where wave-bottom interactions are dominated by Bragg scattering (Figure 12).

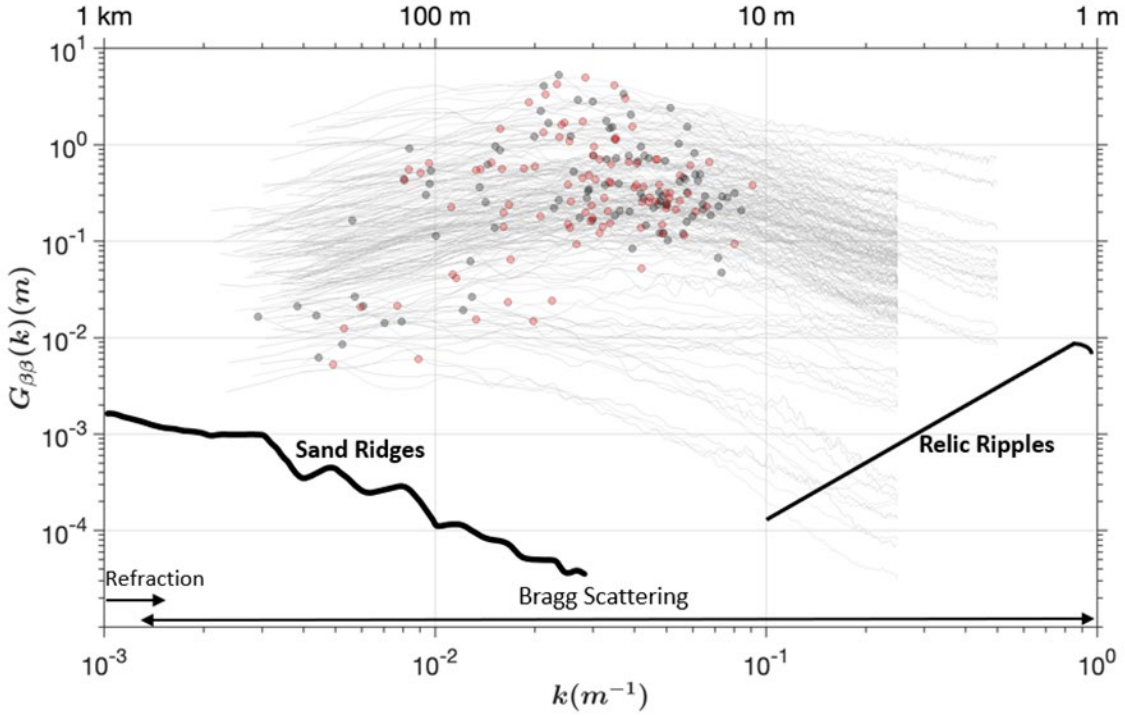

Wave bottom interactions, for different topography scales. The light gray lines are the unnormalized bottom slope spectra (α_β) of the rocky bottom subsets. The location of the maximum variance for each spectrum is indicated for the cross-shore (red dots) and alongshore (black dots). The black lines depicting sand ridges and relic ripples are adapted from Ardhuin et al., 2003.

Figure 12. Wave bottom interactions

THIS PAGE INTENTIONALLY LEFT BLANK

V. CONCLUSION

The bottom roughness of 99 rocky bottom subsets is calculated along the entire California coast from bathymetry data with 1 or 2m resolution obtained from California State University Monterey Bay's Seafloor Mapping Laboratory. The 99 subsets provide a large population to make meaningful statistical inferences. Roughness is defined as the elevation deviation, z', about a mean planform that is averaged over 750m in the alongshore and cross-shore. The <750m is the scale of intermediate wave processes. Visual examination of the rocky bottom z' find them to vary widely in appearance. Measures of roughness include statistical parameters of standard deviation, σ_z, skewness and kurtosis, probability functions, and wavenumber spectra of elevation, $\widehat{G_{zz}}(k)$, and bottom slopes, $\widehat{G_{\beta\beta}}(k)$. σ_z of the rocky bottom subsets vary widely from 0.3-8.6m with an average roughness of 2.1m (Table 1). The measured rocky bottoms are significantly rougher than previously measured roughness for coral reefs ($0.03 < \sigma_z < 0.99$). σ_z and $\widehat{G_{zz}}(k)$ in x and y are similar, suggesting rocky bottoms are isotropic in the cross- and alongshore directions. The $\widehat{G_{zz}}(k)$ spectra are red, with the highest variances at the lowest wave numbers. The bottom slope σ_β are linearly related to bottom roughness σ_z with $\sigma_\beta \propto 0.8\sigma_z$ ($R^2 = 0.75$).

The average spectral slopes of all $\widehat{G_{zz}}(k)$ in x and y, $\widehat{\alpha_z}(k)$, and the average spectral slopes of all $\widehat{G_{\beta\beta}}(k)$ for bottom slopes in x and y, $\widehat{\alpha_\beta}(k)$, are isotropic with their 95% confidence intervals overlapping for the intermediate wave scales <1/666m (Figure 8c,d). The range of spectral slopes of z' are similar to those found in coral reefs (Table 1). The $\widehat{\alpha_z}(k)$ decreases with wavenumber from -1 to -3, the same range found for coral reefs. The spectral shapes of $\widehat{\alpha_z}(k)$ and $\widehat{\alpha_\beta}(k)$ are near identical. A Fourier model is derived for surface elevation and bottom slopes. Assuming the elevation spectra are described by a power law in wavenumber space, it is shown that the slopes of the bottom slopes can be obtained by the spectral transformation $log\ \widehat{\alpha_\beta}(k) = log\ \widehat{\alpha_z}(k)$ +2. The $\widehat{\alpha_\beta}(k)$ obtained by the spectral transformation and $\widehat{\alpha_\beta}(k)$ and from independently measured bottom slopes compare well. Therefore, rocky bottom roughness can be

reasonably described using a Fourier representation. The k at which $\widehat{\alpha_\beta}(k)$ is maximum indicates the scale of the steepest mean slope. The steepest slope is the scale that determines the dominant form drag for bottom dissipation (Rodgers et al., 2018). The length scales where 80% of the maximum slopes occur range from 15 to 80m for rocky bottoms.

LIST OF REFERENCES

Ardhuin, F., T. Drake, and T. Herbers, 2002: Observations of Wave-Generated Vortex Ripples on the North Carolina Continental Shelf. *Journal of Geophysical Research*, **107** https://doi.org/10.1029/2001JC000986.

Ardhuin, F., W. O'Reilly, T. Herbers, and P. Jessen, 2003: Swell transformation across the continental shelf. Part I: Attenuation and directional broadening. *Journal of Physical Oceanography*, **33(9)**, 1921–1939. https://doi.org/10.1175/1520-0485(2003)033<1921:STATCS>2.0.CO;2.

Bird, E., 2011: *Coastal Geomorphology: An Introduction* (2nd ed). John Wiley and Sons, 436 pp.

Brandt, A., and R. Brincker, 2014: Integrating time signals in frequency domain – Comparison with time domain integration. *Measurements*, **58**, 511-519. https://doi.org/10.1016/j.measurement.2014.09.004.

California State University at Monterey Bay(CSUMB) - Seafloor Mapping Lab(SFML), 2016: SFML Data Library, accessed 06 January 2021, http://seafloor.otterlabs.org/SFMLwebDATA.htm.

Duvall, M. S., J.L. Hench, and J.H. Rosman, 2019: Collapsing complexity: Quantifying multiscale properties of reef topography. *Journal of Geophysical Research: Oceans*, **124(7)**, 5021–5038. doi: 10.1029/2018JC014859.

Duvall, M. S., J.H. Rosman, and J.L. Hench, 2020: Estimating geometric properties of coral reef topography using obstacle- and surface-based approaches. *Journal of Geophysical Research: Oceans*, **125**, e2019JC015870. https://doi.org/10.1029/2019JC015870.

Emery, K. O., and G. G. Kuhn, 1982: Sea cliffs: Their processes, profiles, and classification.

Golden, N.E., 2016: California State Waters Map Series Data Catalog. U.S. Geological Survey Data Series 781, accessed 04 September 2022. http://pubs.usgs.gov/ds/781/.

Gon, C. J., J.H MacMahan, E.B. Thornton, and M. Denny, 2020: Wave dissipation by bottom friction on the inner shelf of a rocky shore. *Journal of Geophysical Research: Oceans*, **125**(e2019JC015963). https://doi.org/10.1029/2019JC015963.

Grant, W. D., and O.S. Madsen, 1982: Movable bed roughness in unsteady oscillatory flow. *Journal of Geophysical Research*, **87(C1)**, 469. https://doi.org/10.1029/JC087iC01p00469.

Griggs, G., K. Patsch, and L. Savoy, 2005: *Living with the Changing California Coast*. University of California Press, 540 pp.

Hasselmann, K., and J.I. Collins, 1968: Spectral dissipation of finite-depth gravity waves due to turbulent bottom friction. *Journal of Marine Research*, **26**, 1–12. https://doi.org/10.1007/BF00232479.

Jackson, D.R., and M.D. Richardson, 2007: *High-Frequency Seafloor Acoustics*. Springer, 603pp.

Jaramillo, S., and G. Pawlak, 2011: AUV-based bed roughness mapping over a tropical reef. *Coral Reefs*, **30**, 11-23. doi:10.1007/s00338-011-0731-9.

Johnson, S., G.R. Cochrane, N.E. Golden, P. Dartnell, S.R. Hartwell, S.A. Cochran, and J.T. Watt, 2017: The California Seafloor and Coastal Mapping Program – Providing science and geospatial data for California's State Waters. *Ocean & Coastal Management*, **140**, 88–104. https://doi.org/10.1016/j.ocecoaman.2017.02.004.

Kirk, R. M., 1977: Rates and forms of erosion on intertidal platforms at Kaikoura Peninsula, South Island, New Zealand. *New Zealand Journal of Geology and Geophysics*, **20(3)**, 571–613. doi:10.1080/00288306.1977.10427603.

Lentz, S. J., J.H. Churchill, K.A. Davis, J.T. Farrar, J. Pineda, and V. Starczak, 2016: The characteristics and dynamics of wave-driven flow across a platform coral reef in the Red Sea. *Journal of Geophysical Research: Oceans,* **121(2)**, 1360–1376. doi:10.1002/2015jc011141.

Long, R. B., 1973: Scattering of surface waves by an irregular bottom. *Journal of Geophysical Research*,**78 (33)**, 7861–7870. https://doi.org/10.1029/JC078i033p07861.

Lowe, R. J., J.L. Falter, M.D. Bandet, G. Pawlak, M.J. Atkinson, S.G. Monismith, and J.R. Koseff, 2005: Spectral wave dissipation over a barrier reef. *Journal of Geophysical Research,* **110 (C4)**, https://doi.org/10.1029/2004JC002711.

Monismith, S. G., J.S. Rogers, D. Koweek, and R.B. Dunbar, 2015: Frictional wave dissipation on a remarkably rough reef. *Geophysical Research Letters*, **42**, 4063–4071. https://doi.org/10.1002/2015GL063804.

Nielsen, P., 1992: Coastal bottom boundary layers and sediment transport. *World Scientific*, **340(124)**, 2–20. https://doi.org/10.1142/1269.

Nunes, V. and G. Pawlak, 2008: Observations of Bed Roughness of a Coral Reef. *Journal of Coastal Research*, **24**, 39–50. https://doi.org/10.2112/05-0616.1.

Poate, T., G. Masselink, M.J. Austin, M. Dickson, and R. McCall, 2018: The role of bed roughness in wave transformation across sloping rock shore platforms. *Journal of Geophysical Research: Earth Surface*, **123(1)**, 97–123. doi:10.1002/2017JF004277.

Rogers, J. S., S.A. Maticka, V. Chirayath, C.B. Woodson, J.J Alonso, and S.G. Monismith, 2018: Connecting flow over complex terrain to hydrodynamic roughness on a coral reef. *Journal of Physical Oceanography,* **48(7)**, 1567–1587. https://doi.org/10.1175/JPO-D-18-0013.1.

Soulsby, R., 1997: *Dynamics of Marine Sands*. London, UK: Thomas Telford. 272pp. https://www.icevirtuallibrary.com/isbn/9780727739551.

Thomson, R.E. and W.J. Emery, 2014: *Data analysis methods in physical oceanography* (3rd ed.). Elsevier, 716 pp.

Trenhaile, A. S., 2002: Rock coasts, with particular emphasis on shore platforms. *Geomorphology*, **48** (1-3), 7–22. doi:10.1016/s0169-555x(02)00173-3.

Witman, J.D. and P.K. Dayton, 2001: Rocky subtidal communities. *Marine Community Ecology*, Sinauer Associates, 339-366.

THIS PAGE INTENTIONALLY LEFT BLANK

INITIAL DISTRIBUTION LIST

1. Defense Technical Information Center
   Ft. Belvoir, Virginia

2. Dudley Knox Library
   Naval Postgraduate School
   Monterey, California